PHYSICAL REVIEW A **94**, 061803(R) (2016)

Self-determining high-frequency oscillation from an external-cavity laser diode

Émeric Mercier,[1,2] Chi-Hak Uy,[1,2] Lionel Weicker,[1,2] Martin Virte,[3] Delphine Wolfersberger,[1,2] and Marc Sciamanna[1,2]
[1]*LMOPS, CentraleSupélec, Université Paris-Saclay, 57070 METZ*
[2]*LMOPS, CentraleSupélec, Université de Lorraine, 57070 METZ*
[3]*Vrije Universiteit Brussel, Department of Applied Physics and Photonics, Brussels Photonics (B-PHOT), Pleinlaan 2, B-1050 Brussels, Belgium*

(Received 9 June 2016; published 28 December 2016)

We report on a bifurcation mechanism following which an external-cavity laser diode emits regular oscillating output power at a high frequency. This frequency does not vary with the external-cavity length and it can be adjusted by varying the feedback strength. We observe this phenomenon numerically by investigating the external-cavity modes generated by a semiconductor laser subject to a phase-conjugate optical feedback. Particularly, we explore the effects of both the feedback rate and the time delay induced by the feedback on the frequency of the external-cavity modes. Counterintuitively, we evidence that having a short cavity does not necessarily yield oscillations at higher frequencies. We show that the key parameter in order to generate high-frequency solutions is the feedback rate. This parameter fixes the frequency of the solutions obtained independently of the time delay. We finally relate our observations to Hopf bifurcation phenomena.

DOI: 10.1103/PhysRevA.94.061803

Semiconductor lasers have been studied for several decades due to the richness of their nonlinear dynamics [1,2]. Modulating the injection current, adding feedback, or injecting light from another source can either improve the laser performances or lead to dynamical regimes where the emitted light oscillates regularly or chaotically with time [3,4]. For some time, it has been considered a challenge to make a semiconductor laser oscillate or pulse at frequencies higher than its relaxation oscillation frequency. In a laser with conventional optical feedback (COF), oscillations or pulses at a frequency inversely proportional to the external-cavity length can be obtained [5–11]. The focus was thus put on obtaining ultrashort cavities, which was achieved thanks to distributed feedback lasers where the external cavity is integrated with the laser device [12] and oscillations at high frequency have been unlocked [12,13].

Another approach for unlocking oscillating states in a laser diode is to use phase-conjugate feedback (PCF). It has been shown that a laser with PCF sustains external-cavity modes (ECMs) which are self-pulsating solutions at harmonics of the external-cavity frequency [14–16], and higher harmonics are unlocked as the feedback rate is increased. The authors of Ref. [16] suggest in their conclusion that reducing the time delay would also contribute to increasing the frequency of oscillations observed. In this Rapid Communication, we show theoretically that the system locks on ECMs of higher harmonics when increasing the external-cavity length at a fixed feedback rate, such that the oscillation frequency remains almost constant. In a laser with PCF, the self-pulsation frequency is thus determined by the feedback rate, independently from the external-cavity length, whereas in a laser with COF regular high-frequency oscillations require shortening the external cavity [7–12,17].

A semiconductor laser subject to instantaneous PCF can be described by the following dimensionless rate equations [14]

$$\dot{Y} = (1 + i\alpha)ZY + \gamma Y^*(t - \theta), \tag{1}$$

$$T\dot{Z} = P - Z - (1 + 2Z)|Y|^2, \tag{2}$$

where $Y(t)$ corresponds to the complex electric field and $Z(t)$ represents the carrier density. The time t is normalized by the photon lifetime τ_p. γ is the dimensionless feedback rate proportional to the square root of the power reflectivity of the phase-conjugate mirror (PCM), α corresponds to the linewidth enhancement factor, θ is the external-cavity round-trip time normalized by τ_p, T is the ratio of carrier to photon lifetimes, and P is the pump parameter above threshold. In this Rapid Communication, we consider the following set of parameter values that have been largely used in the literature [14,15,18–20]: $\alpha = 3$, $T = 1428$, and $P = 0.0417$.

These values correspond to a semiconductor laser operating close to threshold. The range of θ considered in this study is between 1 and 958, or—using $\tau_p = 1.4$ ps—equivalently between 0.0014 and 1.34 ns in real time units. This range is centered around $\theta = 476$, the value considered in several studies that use a fixed time delay [14,15,21]. The upper bound is close to the value used in the experimental observation of ECMs [16]. The multiple delayed round-trips in the external cavity are not taken into account in this model because we are interested in relatively low reflectivities of the external mirror (γ between 0 and 0.05). Moreover, the frequency dependence of the PCM reflectivity and the time for light to traverse the nonlinear medium have also been neglected. The latter assumption is justified since we typically use short crystals (less than 1 cm long) to generate the phase-conjugate signal [22–24]. Later on, we demonstrate that accounting for the crystal finite penetration length does not modify our conclusions.

We explore the effects of both the delay θ and the feedback strength γ on the ECMs. To this end, we use a fourth order Runge-Kutta algorithm to compute time traces from which we create a bifurcation diagram of the output power versus the feedback rate γ for a given value of the time delay θ. Figure 1(a) shows a bifurcation diagram obtained for $\theta = 400$. The typical behavior of a laser with PCF is observed, i.e., a stable steady state for a very low feedback rate, followed by a Hopf bifurcation leading to undamped oscillations at the relaxation frequency of the laser and then a succession of

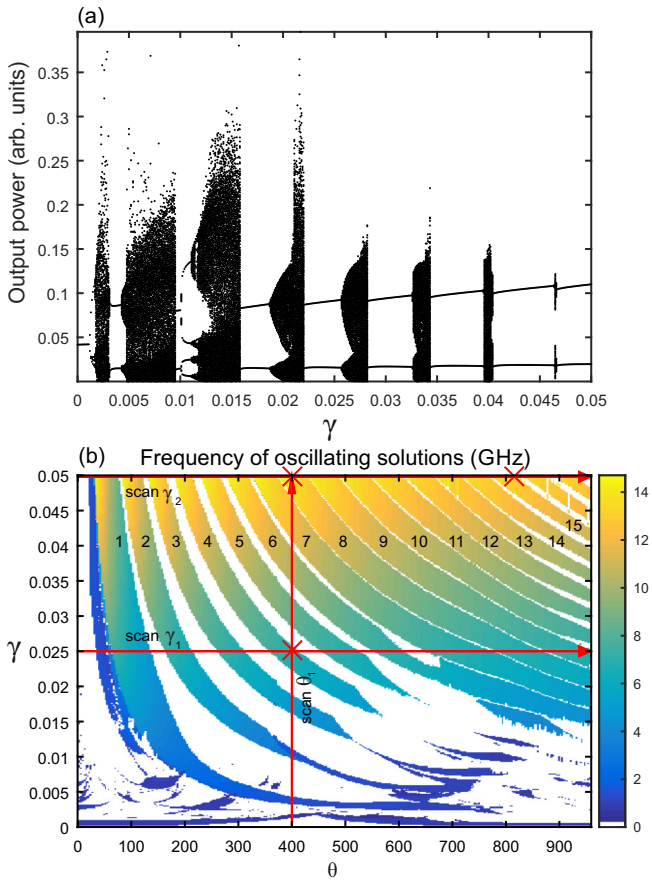

FIG. 1. (a) Bifurcation diagram corresponding to the extrema of the output power with γ as the bifurcation parameter. The bifurcation diagram has been obtained from Eqs. (1) and (2) with the values of the parameters fixed to $P = 0.0417$, $\theta = 400$, $T = 1428$, and $\alpha = 3$. (b) Mapping of periodic solutions in the parameter plane (θ, γ). The color bar on the right indicates the frequency of oscillations in GHz. The orders of ECMs are labeled on the bands of hyperbolic shape and the red arrows and crosses serve as indicators for Figs. 2 and 3.

bifurcations corresponding to a cascade of different regimes [14,19]. For higher values of γ, the system exhibits successive ECMs interspersed with regions of chaos that shrink as γ increases [15].

From this bifurcation diagram and the associated time traces, we identify the oscillating solutions and measure their frequencies, discarding steady states, quasiperiodic solutions, and chaos. We repeat the process for values of the time delay in the aforementioned range and report the measured frequency of oscillations in Fig. 1(b), color-coded in the plane (θ, γ). The white background corresponds to regions where the dynamics have been discarded (nonoscillating solutions). Each band in the map corresponds to a unique ECM of order n [numerical labels in Fig. 1(b)], meaning that its frequency is equal to n times the external-cavity frequency $f_{EC} = 1/(\theta\tau_p)$. The oscillating frequency of the ECM of order n is therefore given by $f_n = n/(\theta\tau_p)$. The undamping of relaxation oscillations is observed in the bottom of the map for low values of γ. The darkest shade of blue identifies parameter regions where the laser shows regular self-pulsation at a frequency close to the frequency of relaxation oscillations, varying from

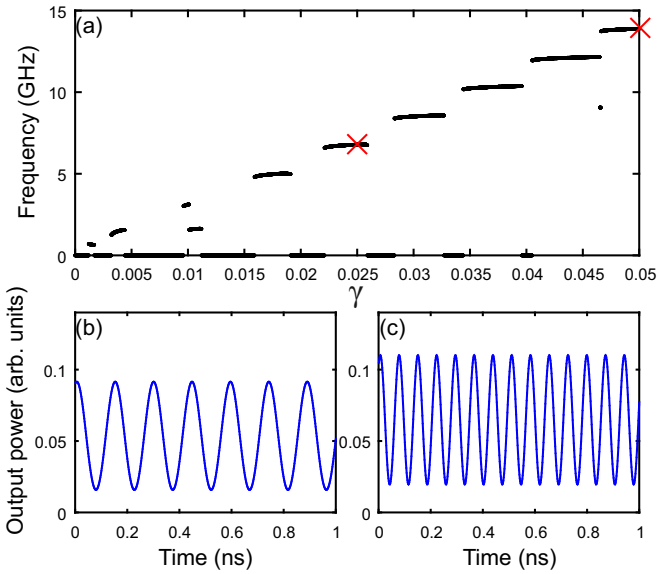

FIG. 2. (a) Frequency of the time-periodic regimes for $\theta = 400$ as a function of the feedback rate. (b) and (c) are the time series of the output power for $\gamma = 0.025$ and $\gamma = 0.05$, respectively. Other parameters are the same as in Fig. 1(a).

750 MHz to 1 GHz—with $\tau_p = 1.4$ ps—depending on the values of γ and θ.

We then explore the map by scanning it along different directions [see red arrows in Fig. 1(b)]. First, we look at the evolution of the oscillation frequency as a function of the feedback rate with a fixed time delay $\theta = \theta_1 = 400$ [vertical red line in the map of Fig. 1(b)] [see Fig. 2(a)]. We observe that the frequency of oscillations is close to the harmonics of $f_{EC} = 1.78$ GHz, as expected from the literature [15,16]. Increasing the feedback rate leads to the successive stepwise increase of the frequencies. The system visits a significant number of ECMs of higher order, which is illustrated with the time traces in Figs. 2(b) and 2(c), corresponding to the red crosses in Fig. 2(a).

In Fig. 3, we represent the frequency of the oscillations as a function of θ for two fixed values of γ ($\gamma = \gamma_1 = 0.025$ in gray and $\gamma = \gamma_2 = 0.05$ in black). It corresponds to horizontal scans of the map in Fig. 1(b) (see red lines). We first observe that for a slight increase of the delay, the frequency of the oscillations decreases. When the time delay is increased further, we observe that the oscillation frequency goes back up to values close to where it started, which corresponds to a jump to an ECM of higher order. This pattern repeats itself along the θ axis. In the end, the oscillation frequency tends to a constant value when increasing the time delay. Figures 3(b) and 3(c) represent time traces for different values of θ but with γ fixed. We observe that the system generates oscillations of about the same frequency although the external-cavity length doubles from panel (b) to panel (c).

This property is unique and counterintuitive in comparison to what is known from the literature for external-cavity laser diodes [5,7]. For comparison, we plot in Fig. 3(a) (in blue with symbol $\diamond$) the evolution of the frequency for the stable and regular oscillations in the output power of a laser diode subject to COF and $\gamma = 0.025$, all other parameters remaining

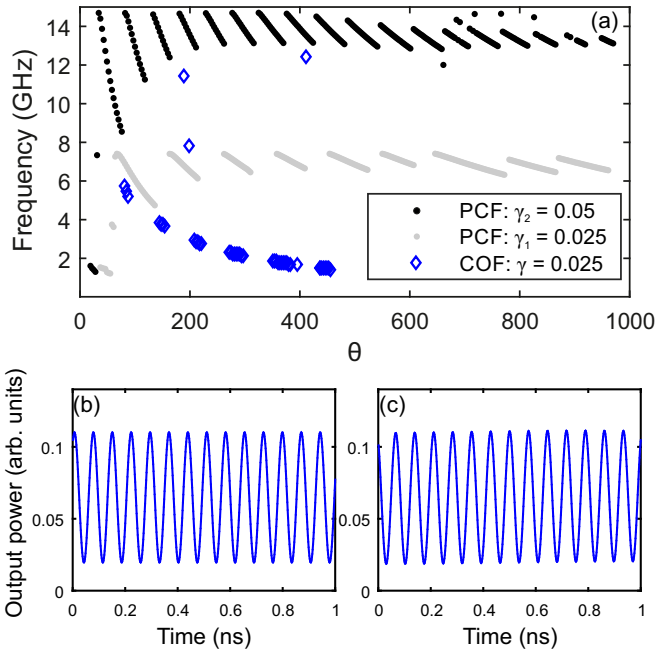

FIG. 3. (a) Frequency of the periodic oscillations for $\gamma_1 = 0.025$ (gray) and $\gamma_2 = 0.05$ (black) as a function of θ for a laser subject to PCF. In blue with diamonds ($\diamond$), the frequency of the periodic oscillations for $\gamma_1 = 0.025$ as a function of θ for a laser subject to COF. (b) and (c) are the time series of the output power for $\theta = 400$ and $\theta = 815$, respectively, in the PCF configuration. Values of the other parameters are the same as in Fig. 2(a) except $\gamma = 0.05$.

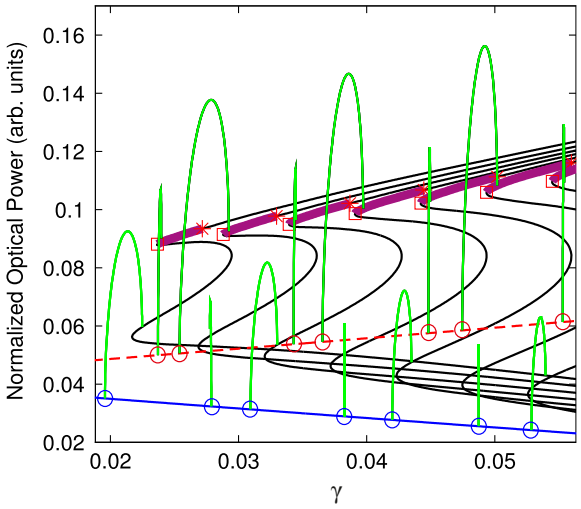

FIG. 4. Bifurcation diagram obtained by continuation. Black lines are the maxima of ECM branches, red (dashed) lines and blue (solid) lines at the bottom are the upper and lower steady-state branches, respectively. Green (gray solid) lines correspond to the periodic solution branches linking the ECM to the steady-state branches by Hopf bifurcation. Circles (◯) are Hopf bifurcations emerging from the steady states. Squares (□) are saddle-node bifurcations and stars (∗) are torus bifurcations. The purple (thick solid) lines represent the areas where the ECM is stable. $\theta = 476$ and the other parameters are the same as in Fig. 1(a).

the same as for the PCF case. In the COF case, a short cavity is more likely to yield the highest possible frequency of regular oscillation. In the PCF configuration instead, a short cavity can slightly increase the frequency but the ruling parameter is the feedback rate. It means that faster oscillations are attainable in the system by increasing the reflectivity of the PCM, regardless of the cavity length.

To summarize this result, we can say that the value of γ approximately sets a particular value for the frequency of oscillation (f_γ) of the laser with PCF. The system will naturally find the order n of ECM that allows $f_n = n/(\theta\tau_p)$ to be the closest possible to f_γ. In addition, f_γ increases monotonously with γ. In order to provide a possible origin for this behavior, we study the Hopf bifurcations of our system, and how the ECM solutions emerge from them.

To this end, we investigate Eqs. (1) and (2) using a continuation method [25] with θ fixed to 476 (see Fig. 4). The system admits two steady states that we call upper (red dashed line) and lower (blue solid line) steady states. The Hopf bifurcations emerging from the steady-state branches are marked by circles (◯). Note that we only consider the interval of feedback strength [0.018; 0.056], for clarity, but other Hopf bifurcations exist outside this interval. The black curves correspond to the maxima of the different ECMs and the purple (thick solid) lines correspond to the regions where they are stable. They are delimited by squares (□) and stars (∗) which are saddle-node and torus bifurcations, respectively. Green (gray solid) lines represent periodic solution branches that link the ECM to the steady-state branches by Hopf bifurcations. We observe that each branch of ECM is connected to two Hopf bifurcations: one from the upper steady state and one from the lower steady state.

From the direct numerical simulations, we are mostly interested in the effect of time delay rather than the feedback strength. Since the ECMs exist through Hopf bifurcations, it is worthwhile to study the Hopf bifurcations and their frequencies in the parameter plan (θ, γ). To this end, we consider the Hopf bifurcation conditions derived in Ref. [14] [Eqs. (B8) and (B9)] and use the Newton-Raphson method in order to find the different Hopf branches. We then follow each branch in the range of feedback strength and delay previously mentioned and obtain Fig. 5(a). Red shows the Hopf bifurcation points emerging from the upper steady-state branch and blue from the lower steady-state branch.

In comparison with Fig. 1(b), we first observe that the shape of the Hopf bifurcation branches follows the shape of the ECM bands. Second, the total number of Hopf bifurcations emerging from the upper and lower steady-states is approximately twice the number of ECMs, which is consistent with our observation in Fig. 4.

Of particular interest is the frequency of the Hopf bifurcations. In Fig. 5(b), we represent the Hopf bifurcation frequencies at two given values of γ (0.025 in gray and 0.05 in black). The circles correspond to the one emerging from the lower steady state, whereas the crosses correspond to the upper steady state. As observed for the ECM frequencies [see Fig. 3(a)], the value of γ sets the frequency. For example, when $\gamma = 0.025$, the frequency of the Hopf bifurcations is around 7.5 GHz, whereas when $\gamma = 0.05$ the frequency is around 15 GHz. Note that some of the Hopf bifurcation frequencies

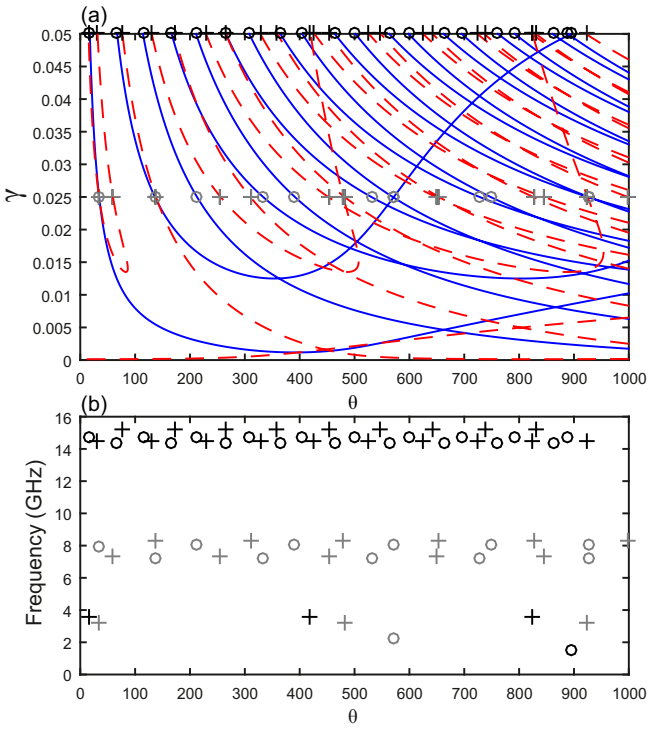

FIG. 5. (a) Hopf bifurcation points emerging from the upper steady-state branch (red dashed lines) and from the lower steady-state branch (blue full lines) in the (θ,γ) plan. Values of the parameters are the same as in Fig. 1(a). (b) Hopf bifurcation frequency as a function of θ. Crosses (+) correspond to the Hopf bifurcation points emerging from the upper steady state, whereas circles (○) correspond to the lower steady state. Gray and black colors correspond to $\gamma_1 = 0.025$ and $\gamma_2 = 0.05$, respectively. Other parameters are the same as in Fig. 1(b).

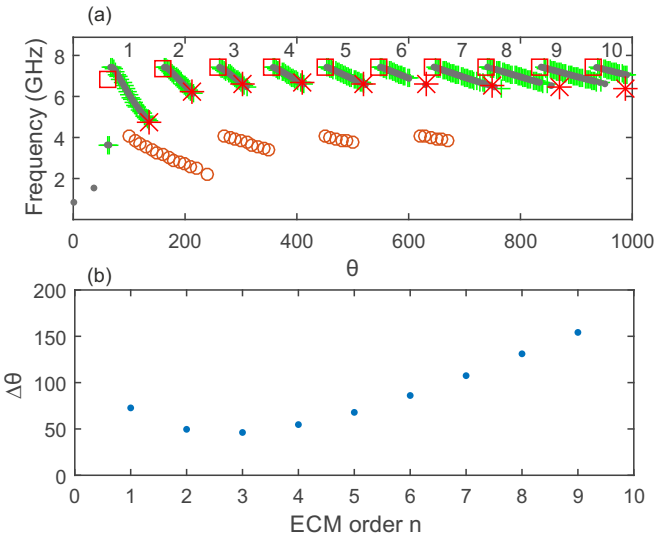

FIG. 6. (a) Gray dots: Frequency of the periodic oscillations for $\gamma_1 = 0.025$ without noise. The labels correspond to the external-cavity mode order. □ and ∗ are saddle-node and torus bifurcations, respectively. Green crosses: Frequency of the periodic oscillations for $\gamma_1 = 0.025$ with spontaneous emission noise. Orange circles: Frequency of the periodic oscillations using the filtered PCF model of Ref. [23] with parameters $P = 0.005$, $\tau_r = 50$, and $\alpha = 3.3$. (b) Evolution of the range of θ leading to stable ECM, labeled $\Delta\theta$ as a function of n, the external-cavity mode order.

exist at low values. They appear when a branch of Hopf bifurcation in the (θ,γ) plan folds back. These values are close to those found for the ECMs. Indeed, for comparison, Fig. 6(a) shows the evolution of the frequency of ECMs as a function of θ (gray dots). The symbols □ and ∗ indicate the saddle-node and torus bifurcations delimiting the stability of the ECMs, as indicated in Fig. 5(a). The feedback rate γ sets the value of the oscillation frequency and that value is close to that obtained from the inspection of the Hopf bifurcation frequencies. Moreover, that picture explains why high order ECMs, i.e., ECMs of higher harmonic frequencies, remain stable when increasing θ, hence allowing for the laser self-pulsation frequency to remain constant in spite of the increase of external-cavity length. The stability of ECMs is indeed determined by the saddle-node and torus bifurcations and these bifurcations define a range of θ for which the ECM is stable, labeled $\Delta\theta$ in Fig. 6(b), which increases when increasing θ. This mechanism that explains the stability of ECMs in PCF leads to the self-determining frequency mechanism and also to multistability between ECMs. The increased stability of ECMs when increasing the time delay θ for the PCF case is an opposite conclusion to the one typically retrieved from the long-delay limit analysis of time-delay systems [26,27].

Finally, we have checked whether our theoretical prediction of a self-determining self-pulsation frequency in PCF still holds in situations closer to experimental realizations. In particular, we consider two situations: (i) adding spontaneous emission noise in models (1) and (2) or (ii) accounting for the finite penetration depth in the nonlinear medium as typically observed in experiments using photorefractive crystals. Spontaneous emission is modeled by adding a term $\sqrt{R}\xi(t)$ in Eq. (1) [20,28] modeling a white Gaussian noise of variance R and mean zero. For realistic values of R such as $R = 10^{-12}$ (corresponding to $D = 10^{-4}$ ns^{-1} in Ref. [28]), the model predicts that the jumps between ECMs may occur at slightly different values of θ and in a slightly more erratic way. As shown in Fig. 6(a) (green "+" symbols) the self-pulsation frequency shows a similar evolution with θ as in the deterministic case. The inclusion of the photorefractive crystal penetration depth is done as in Ref. [23] with an additional filter equation on the feedback field. The orange circles in Fig. 6(a) show the evolution of the self-pulsing frequency for parameters $P = 0.005$, $\tau_r = 50$ meaning a crystal about 5 mm long with a refractive index equal to 2.1, $\alpha = 3.3$. Since this filtering effect leads to restabilization of the laser dynamics for large γ, the regime of ECM is shifted to lower γ. The situation shown in Fig. 6(a) is for a lower feedback rate ($\gamma = 0.019$) and hence leads to a lower self-pulsating frequency, which is consistent with our previous analysis.

In summary, we have reported a counterintuitive phenomenon in external-cavity laser diodes. In order to generate high-frequency solutions, we usually consider very small external cavities, a challenge which has been tackled with on-chip integration. However, in the case of a laser with PCF, unlocking

high-frequency oscillating states can be achieved over a large range of external-cavity lengths. Indeed, we have found that the system self-determines its favored oscillating frequency based on the feedback rate, with only small variations when varying the length of the external cavity. Furthermore, we explain this property by a bifurcation analysis and relate it to Hopf bifurcations from which emerge the oscillating solutions. Our conclusion is robust against the addition of noise or when taking into account the penetration depth of the laser beam in the nonlinear medium constituting the phase-conjugate mirror.

E.M., C.H.U., L.W., D.W., and M.S. acknowledge the support of Conseil Régional de Lorraine, of Préfecture de Lorraine through the projects PHOTON (FEDER) and APOLLO (FEDER/FNADT), of Agence Nationale de la Recherche (ANR) through the TINO project (ANR-12-JS03-005), and of the interuniversity Attraction Poles program of the Belgian Science Policy Office (IAP P7-35 photonics@be). M.V. acknowledges support from the METHUSALEM program of the Flemish Government and the Research Foundation Flanders (FWO).

[1] C. Risch and C. Voumard, J. Appl. Phys. **48**, 2083 (1977).
[2] G. H. M. v. Tartwijk and D. Lenstra, Quantum Semiclassical Opt. **7**, 87 (1995).
[3] J. Sacher, D. Baums, P. Panknin, W. Elsässer, and E. O. Göbel, Phys. Rev. A **45**, 1893 (1992).
[4] M. Sciamanna and K. A. Shore, Nat. Photonics **9**, 151 (2015).
[5] R. F. Broom, Electron. Lett. **5**, 571 (1969).
[6] K. Ikeda, K. Kondo, and O. Akimoto, Phys. Rev. Lett. **49**, 1467 (1982).
[7] A. A. Tager and K. Petermann, IEEE J. Quantum Electron. **30**, 1553 (1994).
[8] E. A. Avrutin, E. L. Portnoi, and J. H. Marsh, IEE Proc: Optoelectron. **147**, 251 (2000).
[9] T. Heil, I. Fischer, W. Elsäßer, and A. Gavrielides, Phys. Rev. Lett. **87**, 243901 (2001).
[10] T. Heil, I. Fischer, W. Elsäßer, B. Krauskopf, K. Green, and A. Gavrielides, Phys. Rev. E **67**, 066214 (2003).
[11] O. Ushakov, S. Bauer, O. Brox, H.-J. Wünsche, and F. Henneberger, Phys. Rev. Lett. **92**, 043902 (2004).
[12] O. Brox, S. Bauer, M. Radziunas, M. Wolfrum, J. Sieber, J. Kreissl, B. Sartorius, and H.-J. Wünsche, IEEE J. Quantum Electron. **39**, 1381 (2003).
[13] B. Pan, L. Yu, D. Lu, L. Zhang, and L. Zhao, Chin. Opt. Lett. **12**, 110605 (2014).
[14] T. Erneux, A. Gavrielides, K. Green, and B. Krauskopf, Phys. Rev. E **68**, 066205 (2003).
[15] M. Virte, A. Karsaklian Dal Bosco, D. Wolfersberger, and M. Sciamanna, Phys. Rev. A **84**, 043836 (2011).
[16] A. Karsaklian Dal Bosco, D. Wolfersberger, and M. Sciamanna, Appl. Phys. Lett. **105**, 081101 (2014).
[17] A. Tabaka, K. Panajotov, I. Veretennicoff, and M. Sciamanna, Phys. Rev. E **70**, 036211 (2004).
[18] G. R. Gray, D. Huang, and G. P. Agrawal, Phys. Rev. A **49**, 2096 (1994).
[19] B. Krauskopf, G. R. Gray, and D. Lenstra, Phys. Rev. E **58**, 7190 (1998).
[20] É. Mercier, D. Wolfersberger, and M. Sciamanna, Opt. Lett. **39**, 4021 (2014).
[21] G. P. Agrawal and J. T. Klaus, Opt. Lett. **16**, 1325 (1991).
[22] D. H. DeTienne, G. R. Gray, G. P. Agrawal, and D. Lenstra, IEEE J. Quantum Electron. **33**, 838 (1997).
[23] L. Weicker, T. Erneux, D. Wolfersberger, and M. Sciamanna, Phys. Rev. E **92**, 022906 (2015).
[24] L. Weicker, T. Erneux, D. Wolfersberger, and M. Sciamanna, Proc. SPIE 9892, Semiconductor Lasers and Laser Dynamics VII, 98920K (2016).
[25] K. Engelborghs, T. Luzyanina, and G. Samaey, DDE-BIFTOOL v. 2.00: A Matlab Package for Bifurcation Analysis of Delay Differential Equations, Technical Report No. TW-330, Department of Computer Science, K. U. Leuven, Belgium, 2001 (unpublished).
[26] J. Sieber, M. Wolfrum, M. Lichtner, and S. Yanchuk, Discrete Contin. Dyn. Syst. A **33**, 3109 (2013).
[27] D. Puzyrev, S. Yanchuk, A. Vladimirov, and S. Gurevich, SIAM J. Appl. Dyn. Syst. **13**, 986 (2014).
[28] J. Zamora-Munt, C. Masoller, and J. García-Ojalvo, Phys. Rev. A **81**, 033820 (2010).